Human Molecular Genetics, 2018, Vol. 27, No. 6 1093–1105

doi: 10.1093/hmg/ddy031
Advance Access Publication Date: 17 January 2018
Original Article

ORIGINAL ARTICLE

Regulation of ciliary function by fibroblast growth factor signaling identifies FGFR3-related disorders achondroplasia and thanatophoric dysplasia as ciliopathies

Michaela Kunova Bosakova[1], Miroslav Varecha[1,2], Marek Hampl[3,4], Ivan Duran[5], Alexandru Nita[1], Marcela Buchtova[3,4], Hana Dosedelova[4], Radek Machat[3,4], Yangli Xie[6], Zhenhong Ni[6], Jorge H. Martin[5], Lin Chen[6], Gert Jansen[7], Deborah Krakow[5,8,9] and Pavel Krejci[1,2,*]

[1]Department of Biology, Faculty of Medicine, Masaryk University, 62500 Brno, Czech Republic, [2]International Clinical Research Center, St. Anne's University Hospital, 65691 Brno, Czech Republic, [3]Institute of Experimental Biology, Faculty of Sciences, Masaryk University, 62500 Brno, Czech Republic, [4]Institute of Animal Physiology and Genetics, Czech Academy of Sciences, 60200 Brno, Czech Republic, [5]Department of Orthopaedic Surgery, David Geffen School of Medicine at UCLA, Los Angeles, CA 90095, USA, [6]Department of Rehabilitation Medicine, Third Military Medical University, Chongqing 400042, China, [7]Department of Cell Biology, Erasmus MC, 3000 CA Rotterdam, The Netherlands, [8]Department of Human Genetics and [9]Department of Obstetrics and Gynecology, David Geffen School of Medicine at UCLA, Los Angeles, CA 90095, USA

*To whom correspondence should be addressed at: Department of Biology, Faculty of Medicine, Masaryk University, Kamenice 5, 62500 Brno, Czech Republic. Tel: +420 549495395; Fax: +420 549491327; Email: krejcip@med.muni.cz

Abstract

Cilia project from almost every cell integrating extracellular cues with signaling pathways. Constitutive activation of FGFR3 signaling produces the skeletal disorders achondroplasia (ACH) and thanatophoric dysplasia (TD), but many of the molecular mechanisms underlying these phenotypes remain unresolved. Here, we report *in vivo* evidence for significantly shortened primary cilia in ACH and TD cartilage growth plates. Using *in vivo* and *in vitro* methodologies, our data demonstrate that transient versus sustained activation of FGF signaling correlated with different cilia consequences. Transient FGF pathway activation elongated cilia, while sustained activity shortened cilia. FGF signaling extended primary cilia via ERK MAP kinase and mTORC2 signaling, but not through mTORC1. Employing a GFP-tagged IFT20 construct to measure intraflagellar (IFT) speed in cilia, we showed that FGF signaling affected IFT velocities, as well as modulating cilia-based Hedgehog signaling. Our data integrate primary cilia into canonical FGF signal transduction and uncover a FGF-cilia pathway that needs consideration when elucidating the mechanisms of physiological and pathological FGFR function, or in the development of FGFR therapeutics.

Received: October 23, 2017. **Revised:** January 8, 2018. **Accepted:** January 9, 2018

Introduction

Primary cilium is a microtubule-based organelle projecting from the cytoplasm of most post-mitotic vertebrate cells, integrating signal transduction and enabling cell-to-cell communication. The production and maintenance of primary cilia depend on intraflagellar transport (IFT) which moves protein cargo alongside the axoneme (the microtubule skeleton of cilia) towards the tip (anterograde IFT, IFTB) and back to the basis of the cilia (retrograde IFT, IFTA). The anterograde IFT motor is a trimeric kinesin 2 molecule comprised of kinesins KIF3A and KIF3B, and the associated protein KAP3, while retrograde transport is mediated by the dynein motor containing heavy and light intermediate dyneins DYNC2H1 and DYNC2LI1 (1). At least 22 distinct IFTB and IFTA complex proteins participate in IFT that mediate carefully orchestrated entry of ciliary proteins via the transition zone at the base of primary cilia, docking for anterograde IFT, unloading at the ciliary tip and docking for transport out of the cilia (2).

In vertebrates, the signaling of Hedgehog (Hh) family of growth factors and morphogens depends on the primary cilium, as evidenced by defects in Sonic hedgehog (Shh)-mediated neural tube patterning in mice with disrupted ciliogenesis due to genetic ablation of *Kif3a* or mutations in IFTB complex proteins IFT88 and IFT172 (3). Hh signals through its receptor Patched (PTCH) localized in the cilium and in the absence of ligand prevents the activator component of Hh pathway, Smoothened (SMO), from entering the cilia (4). Upon Hh ligand binding to PTCH, SMO enters into the cilium to promote proteolytic processing of the transcriptional regulators from the Glioma (GLI) family, which are transported out of cilia to regulate downstream gene transcription (5). Three members of GLI family differ in Hh-mediated transcriptional modulation. GLI2 and GLI3 form both full-length transcriptional activators and cleaved transcriptional repressor forms, while GLI1 functions solely as a full-length activator (6). Genetic analyses demonstrated that GLI3 is the primary effector of Hh-mediated limb patterning (7).

Four fibroblast growth factor receptors (FGFR1–4) are transmembrane tyrosine kinases that respond to 18 FGF ligands, delivering cell instructions critical for proper development, regeneration and maintenance of tissue homeostasis (8). Dysregulated FGFR signaling underlies several types of skeletal disorders, including craniosynostoses syndromes and skeletal dysplasias. Activating mutations of FGFR3 produce achondroplasia (ACH), the most prevalent nonlethal human dwarfing condition and thanatophoric dysplasia (TD), the most common lethal skeletal dysplasia. Activating mutations in FGFR3 also account for hypochondroplasia and SADDAN syndrome (9). Constitutively active FGFR3 disturbs bone growth via interference with proliferation and differentiation of growth plate chondrocytes (10). The molecular mechanisms underlying these phenotypes are incompletely characterized, complicating our understanding of FGFR3 function and the progress towards rational treatment of ACH. Abnormal Hh signaling accompanies FGFR3-related skeletal dysplasias (11), but the mechanism of this molecular finding remains unclear.

In this study, we report that FGF signaling affects the length of primary cilia, IFT velocities and cilia-based Hedgehog signaling *in vitro* and *in vivo*. Furthermore, we demonstrate a primary cilia defect in ACH and TD *in vivo*, suggesting that deregulation of primary cilia participates in molecular pathology of developmental disorders caused by activating FGFR3 mutations.

Results

Sustained activation of FGF signaling results in shortening of primary cilia

We used previously described ACH mice with heterozygosity for the p.G369C substitution in the gene encoding *Fgfr3* (12) to determine the effect of aberrant FGFR3 activation on primary cilia length. The cilia in the histological sections of tibial growth plate cartilages were visualized by acetylated tubulin immunostaining, and their length measured in 3D. Significantly shorter cilia were found in P1, P3 and P5 ACH mice, compared with wild-type littermates (mean length at P1 ± SEM, 1.19 ± 0.02 μm ACH vs. 1.40 ± 0.02 μm in control, $P < 0.001$) (Fig. 1A). Expression of the constitutively active FGFR3 mutant (p.K650E) associated with TD in NIH3T3 cells also resulted in significant cilia shortening compared with control cells or those expressing wildtype FGFR3 (Fig. 1B).

Similar to NIH3T3 cells expressing the FGFR3 TD mutation (p.K650E), shortening of cilia was observed in cultured human chondrocytes isolated from the cartilage growth plate of TD patients. Treatment of two control and two TD chondrocyte cell lines with the chemical FGFR inhibitor, AZD4547 (13), restored the TD cilia length to the size comparable to control chondrocytes (Fig. 1C). Finally, we observed significantly shorter ($P < 0.001$) primary cilia in TD chondrocytes *in vivo*, derived from femoral growth plate sections obtained from four TD patients, when compared with three independent control growth plates (Fig. 1D).

Figure 1 demonstrates that sustained (strong and constitutive) activation of FGF signaling, by activating mutations in FGFR3, shortens primary cilia *in vitro* and *in vivo*. To test whether a sustained activation of other FGFRs triggers similar phenotype, we determined the effect of FGF signaling on cilia in developing chick limb mesenchyme expressing predominantly FGFR1 (Supplementary Material, Table S1) (14). We injected Hamburger and Hamilton stage 20–22 chick forelimb buds with high concentration of the FGFR1-cognate ligand FGF2 (1 mg/ml) (15) and analysed ciliary length 24 h later. FGF2 produced no effect on cilia length in the posterior limb bud, but progressively shortened cilia were seen in the middle and anterior limb bud regions (Fig. 2A). Finally, we asked whether sustained activation of FGF signaling affects primary cilia in cell systems unrelated to the limb. Human embryonic stem cells (hESC) or induced pluripotent stem cells (hiPSC) express FGFR1–4 (Supplementary Material, Table S1) (16), exhibit a particularly strong response to FGF stimulus and require continuous stimulation with high FGF2 doses for self-renewal and maintenance of stemness (17). Treatment with FGF2 significantly ($P < 0.001$) shortened primary cilia in hESC and hiPSC when compared with untreated cells, while chemical inhibition of high endogenous levels of FGF signaling in hESC and hiPSC (18) extended primary cilia length over the controls (Fig. 2B). Altogether, these data establish that sustained activation of FGF signaling results in shortening of primary cilia.

Transient activation of FGF signaling extends primary cilia

If sustained activation of FGF signaling shortens primary cilia, we asked what may be the effect of transient (low level, time restricted) activation of FGF signaling on primary cilia. NIH3T3 fibroblasts expressing FGFR1 and FGFR2 (Supplementary Material, Table S1) (19) were selected as a model, because

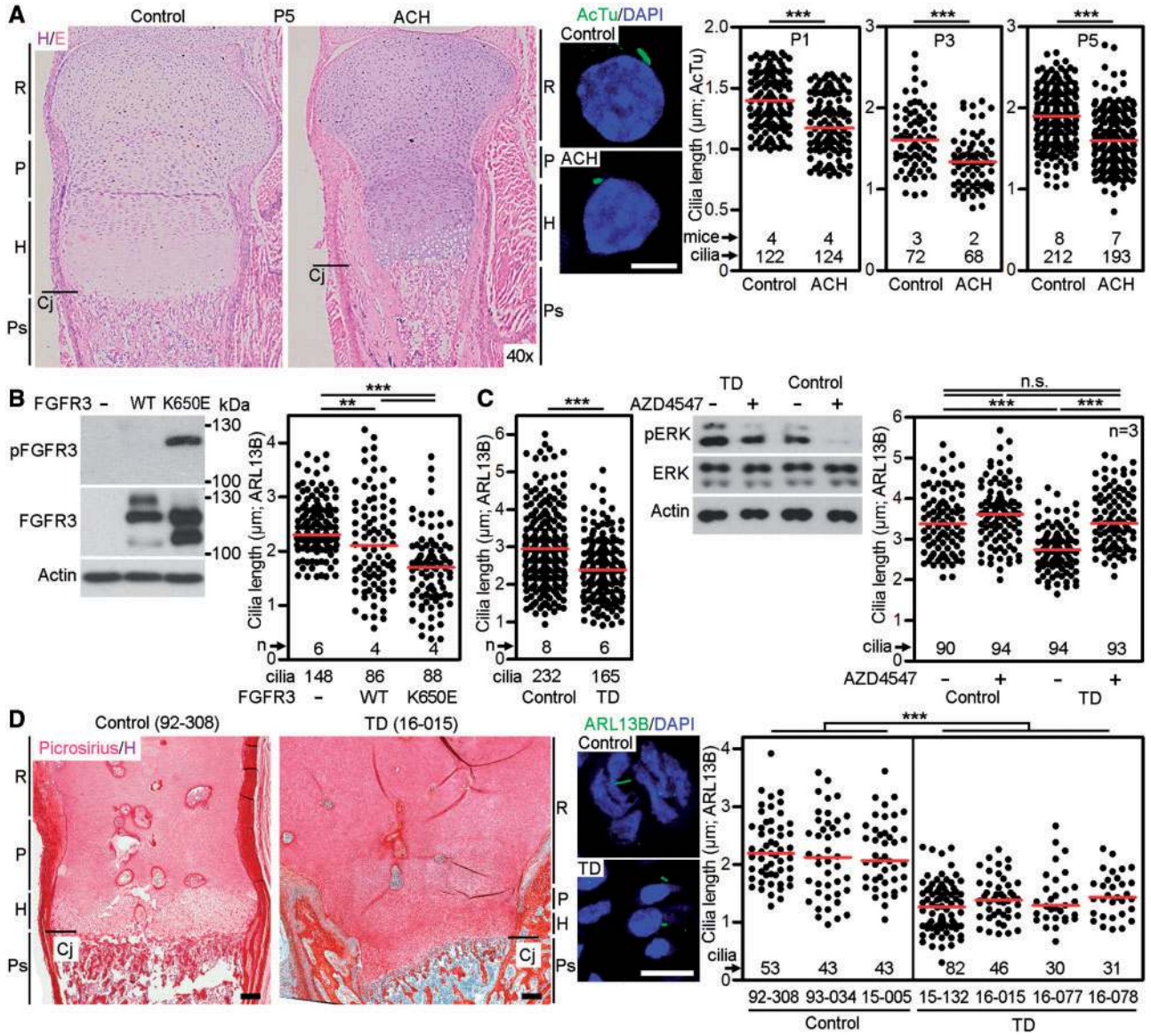

Figure 1. Pathological FGFR3 activation shortened primary cilia *in vivo*. (**A**) Histological representation of tibial growth plate cartilage from control or ACH mice at P5, demonstrating smaller proliferative (P) and hypertrophic (H) zones in ACH (left). Sections were stained with hematoxylin/eosin (H/E). R, resting cartilage; Cj, chondro-osseous junction; Ps, primary spongiosa. Cilia were visualized by immunostaining for acetylated tubulin (AcTu) at P1, P3 and P5, and graphed (middle and right) (scale bar 5 µm; Student's *t*-test, $^{**}P<0.01$, $^{***}P<0.001$). (**B**) NIH3T3 cells were transfected with FLAG-tagged wild type FGFR3 or the constitutively active TD mutant FGFR3-K650E, and analysed for FGFR3 autophosphorylation (p) by western blot, and for cilia length (graph). (**C**) Four control and three TD human chondrocyte cell lines were serum starved and their cilia were measured, compiled and plotted (left). Control (00–082) and TD (97–001) chondrocytes were treated with FGFR3 inhibitor AZD4547 (20 nM) for 12 h. The levels of phosphorylation (p) of the FGFR3 target ERK indicate higher basal levels in TD chondrocytes compared with control (middle). The length of the cilia in controls (90–028, 00–082) and TD chondrocytes (14–005, 97–001) were measured, compiled and plotted (right) (n.s., non-significant). (**D**) Histological representation of control and TD femoral growth plates, showing smaller proliferative and hypertrophic zones in TD. Sections were stained with picrosirius red/hematoxylin (left) (scale bar 50 µm). The cilia in three controls and four TD cartilage growth plates were visualized by ARL13B immunostaining, measured and plotted (middle and right) (scale bar 5 µm).

stimulation of these cells with low levels of FGF ligands leads to transient activation of FGF signaling (20). Cells were serum-starved for 12 h to produce primary cilia, treated with 2 ng/ml of FGF2, and cilia were visualized by immunostainings for the axoneme (acetylated tubulin), ciliary membrane (ARL13B) and centrioles (pericentrin). FGF2 increased cilia length (3.09 ± 0.06 µm vs. 2.33 ± 0.04 µm in controls; mean ± SEM, $P < 0.001$), and this phenotype was rescued by inhibition of FGFR catalytic activity by AZD4547 (Fig. 3A). Similar to NIH3T3 fibroblasts, the primary murine embryonic fibroblasts also showed the FGF2-induced cilia elongation (Fig. 3B). Next, we treated primary micromass cultures of mesenchymal cells established from E12 mouse limb buds with FGF2, and determined the effect on primary cilia (Fig. 3C). Similar to NIH3T3 fibroblasts, FGF2 extended primary cilia in micromass cells expressing predominantly FGFR1 and FGFR2 (Supplementary Material, Table S1) (19). Because NIH3T3 and micromass cells are of mesenchymal origin, we asked whether FGF signaling affects primary cilia also in epithelial cells. Thus, the IMCD3 kidney epithelial cells were treated with epithelial FGF ligands FGF3, FGF7 and FGF10 (21), and the effect

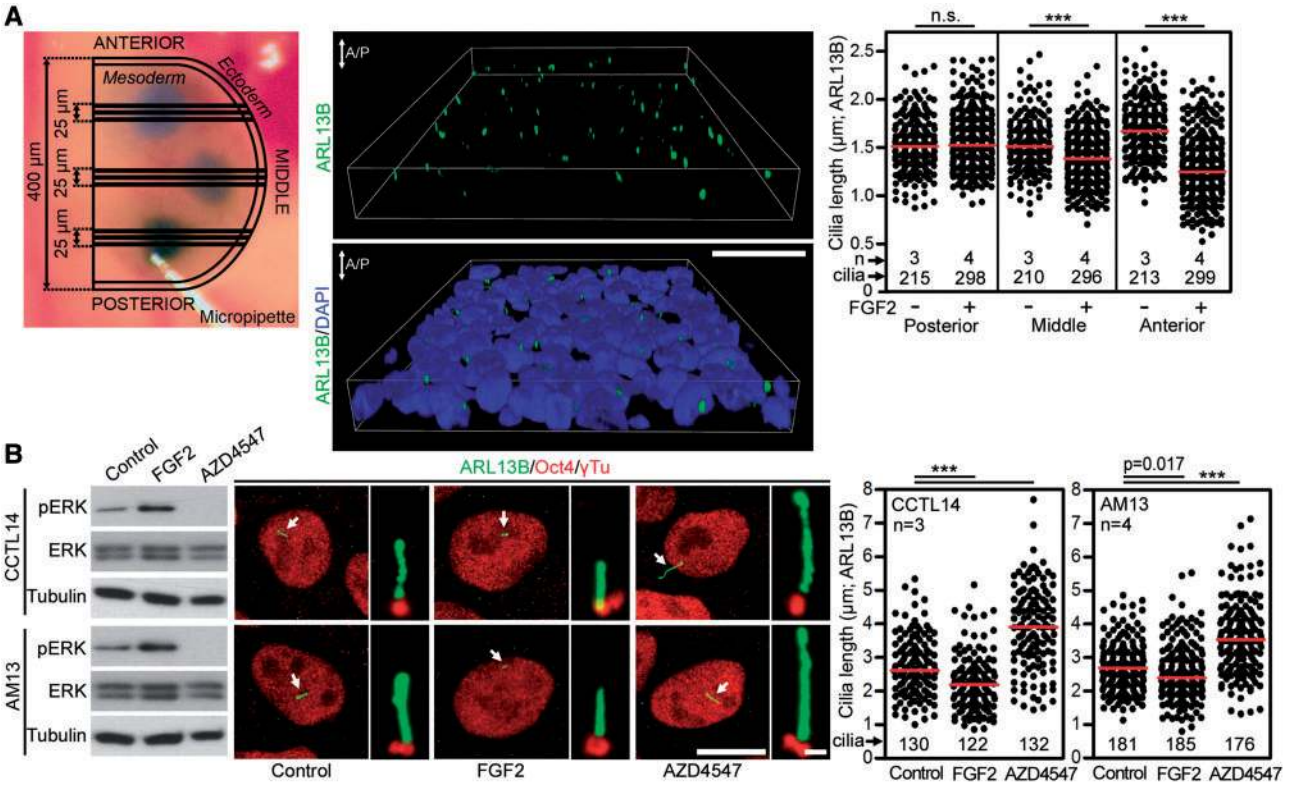

Figure 2. Sustained activation of FGF signaling shortened primary cilia. (**A**) Chick wing buds were injected with either 1 mg/ml FGF2 or vehicle (PBS) for 24 h. Depictions of the limb bud injection sites visualized by trypan blue. Three 5 μm sections from each of the injected sites were analysed (top left). Cilia were visualized by ARL13B immunostaining, measured and graphed (top right; n.s., non-significant). 3D projection of tissue section showing polarized anterior/posterior (A/P) orientation of the cilia (middle). (**B**) Human embryonic stem cells CCTL14 and human induced pluripotent stem cells AM13 were serum starved for 12 h prior treatment with either FGF2 (2 ng/ml) or FGFR inhibitor AZD4547 for 12 h. The FGFR activity was monitored by immunoblot for pERK; ERK and tubulin were used as loading controls (left). Oct4 immunostaining was used as a control of pluripotency (middle). Cilia were visualized using ARL13B and γ-tubulin immunostaining, measured and plotted (middle and right). Scale bars 10 μm (Oct4/ARL13B) and 1 μm (ARL13B/γTu).

of FGF signaling on cilia length was determined. All three FGF ligands caused significant elongation of primary cilia (2.73 ± 0.06 μm in FGF3-treated cells vs. 2.39 ± 0.04 μm in controls; mean ± SEM, $P < 0.001$) (Fig. 3D).

To test whether physiologic, low level FGFR signaling alters cilia *in vivo*, we determined the cilia length in mice where endogenous FGFR signaling was suppressed by systemic treatment with AZD4547, as described in detail elsewhere (19). In the animals treated with AZD4547, significantly shorter cilia ($P < 0.001$) were found in all three examined tissues, that is, the biliary ducts, kidney proximal tubuli and lung bronchi (Fig. 3E), irrespective of their FGFR expression profiles (Supplementary Material, Table S1). Together, these data establish that physiologic levels of FGF signaling or transient FGFR activation extend the length of both motile and primary cilia (Fig. 3F).

FGF signaling extends primary cilia via ERK MAP kinase and mTORC2

To gain insight into the mechanism of FGF-mediated regulation of cilia, NIH3T3 cells were treated with inhibitors of known components of FGFR signal transduction, and the effect on cilia length was determined. Treatment with FGF2 triggered activation of phosphatidylinositol-3-kinase (PI3K)/AKT, mammalian target of rapamycin (mTOR) signaling and ERK MAP kinase signaling in NIH3T3 cells, as evidenced by western blot detection of AKT, p70S6 kinase and ERK phosphorylation (Fig. 4A). Cell treatment with PI828 (PI3K inhibitor) (22) or with mTOR complex 1 (mTORC1) inhibitor rapamycin (23) produced no effect on FGF-mediated cilia extension (Fig. 4B). In contrast, inhibition of ERK pathway by MEK kinase inhibitor PD0325901 (24) partially rescued the FGF-mediated cilia extension without significant effect on cilia length in FGF-naïve cells (Fig. 4B). Similar rescue of FGF-mediated cilia extension was observed in cells treated by AZD3147, a dual inhibitor of mTORC1 and mTORC2 complexes (25) (Fig. 4C). These data suggest a participation of ERK and mTORC2, but not mTORC1 alone, signaling in FGF-mediated regulation of primary cilia.

FGF signaling regulates IFT speed in primary cilia

Because the axoneme growth depends on free tubulins supplied by IFT to the tip of the cilium (26), we asked whether FGF signaling affects IFT. NIH3T3 cells were transfected with GFP-tagged IFT20, which is a component of the IFTB complex and has been used for estimation of both anterograde and retrograde IFT velocities (27). When expressed in NIH3T3 cells, the IFT20-GFP showed a typical IFT20 localization to Golgi and cilium (28), where it shuttled between the basal body and distal tip (Fig. 5A and B). In control cells, IFT20-GFP moved with an average anterograde and retrograde velocities of 0.89 ± 0.17 μm/s (mean ± SD) and 0.34 ± 0.12 μm/s, respectively (Fig. 5C). FGF2 accelerated IFT20-GFP speed by approximately 36% (1.21 ± 0.18 μm/s) in anterograde and 62% (0.55 ± 0.17 μm/s) in retrograde

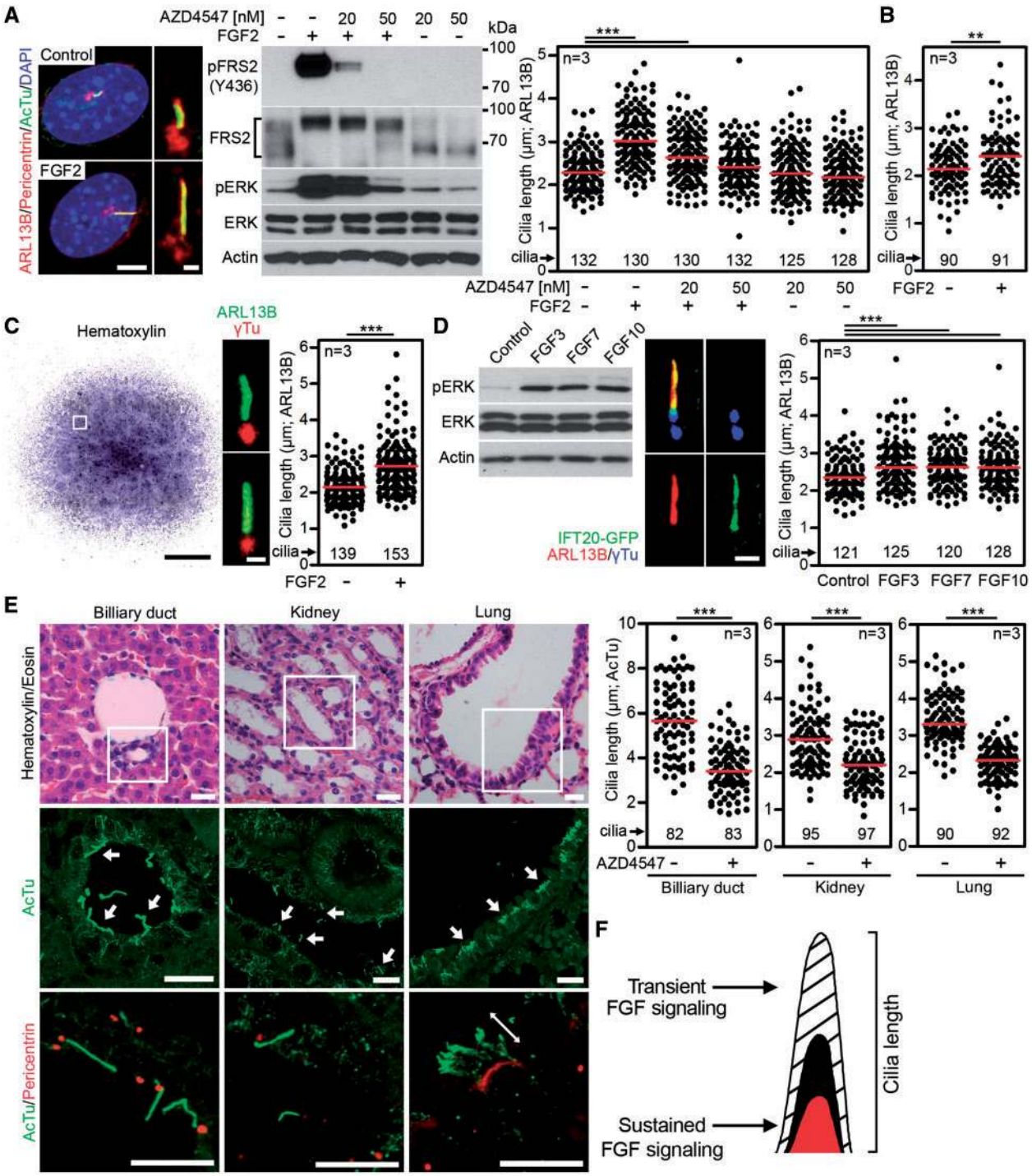

Figure 3. Transient activation of FGF signaling extended primary cilia. (**A**) NIH3T3 cells were treated with FGF2 (2 ng/ml) and FGFR inhibitor AZD4547 for 12 h, and immunostained for the ciliary membrane (ARL13B), axoneme (acetylated tubulin, AcTu), and centrioles (pericentrin). Scale bars 5 μm (left) and 1 μm (right). Cell lysates were immunoblotted for phosphorylation (p) of FRS2 and ERK. Note the marked electrophoretic mobility shift of FRS2 which is due to ERK-mediated phosphorylation. Actin and total levels of FRS2 and ERK served as loading controls. Cilia were visualized by ARL13B immunostaining and their lengths were measured and plotted. Black dots represent individual cilia; red bars show medians (Student's *t*-test, $^{**}P<0.01$, $^{***}P<0.001$). (**B**) Mouse embryonic fibroblasts were serum starved for 12 h prior to treatment with FGF2 (5 ng/ml) for 12 h. Cilia lengths were measured and plotted. (**C**) Micromasses produced from limb buds of E12 mouse embryos were treated with FGF2 (10 or 20 ng/ml) for 24 h and stained with hematoxylin or antibodies for ARL13B and γ-tubulin (γTu). Scale bars 1 mm (micromass) and 1 μm (cilia). The cilia lengths were graphed. (**D**) IMCD3:: IFT20-GFP cells were serum starved for 48 h prior treatment with FGF3, FGF7 or FGF10 (25 or 50 ng/ml) for 12 h. FGFR activity was monitored using pERK immunoblotting; ERK and actin were used as loading controls (left). Cilia were visualized using ARL13B and γTu immunostaining, measured and plotted (middle and right). Scale bar 1 μm. (**E**) Shortened cilia were seen in biliary ducts and proximal kidney tubules, and in multi-ciliated bronchial cells in newborn CD1 mice treated with 1 mM AZD4547 for 28 days (19), compared with AZD4547 vehicle DMSO. Tissue sections were stained with hematoxylin/eosin or antibodies for acetylated tubulin (AcTu) and pericentrin. Arrows point to cilia (scale bars 10 μm). Cilia lengths obtained from three animals were graphed. Black dots represent individual cilia; red bars show medians (Student's *t*-test; $^{***}P<0.001$). (**F**) Model describing how FGF signaling regulates the length of primary cilia. Transient activation of FGF signaling extends the cilia length while constitutive FGF activation shortens primary cilia.

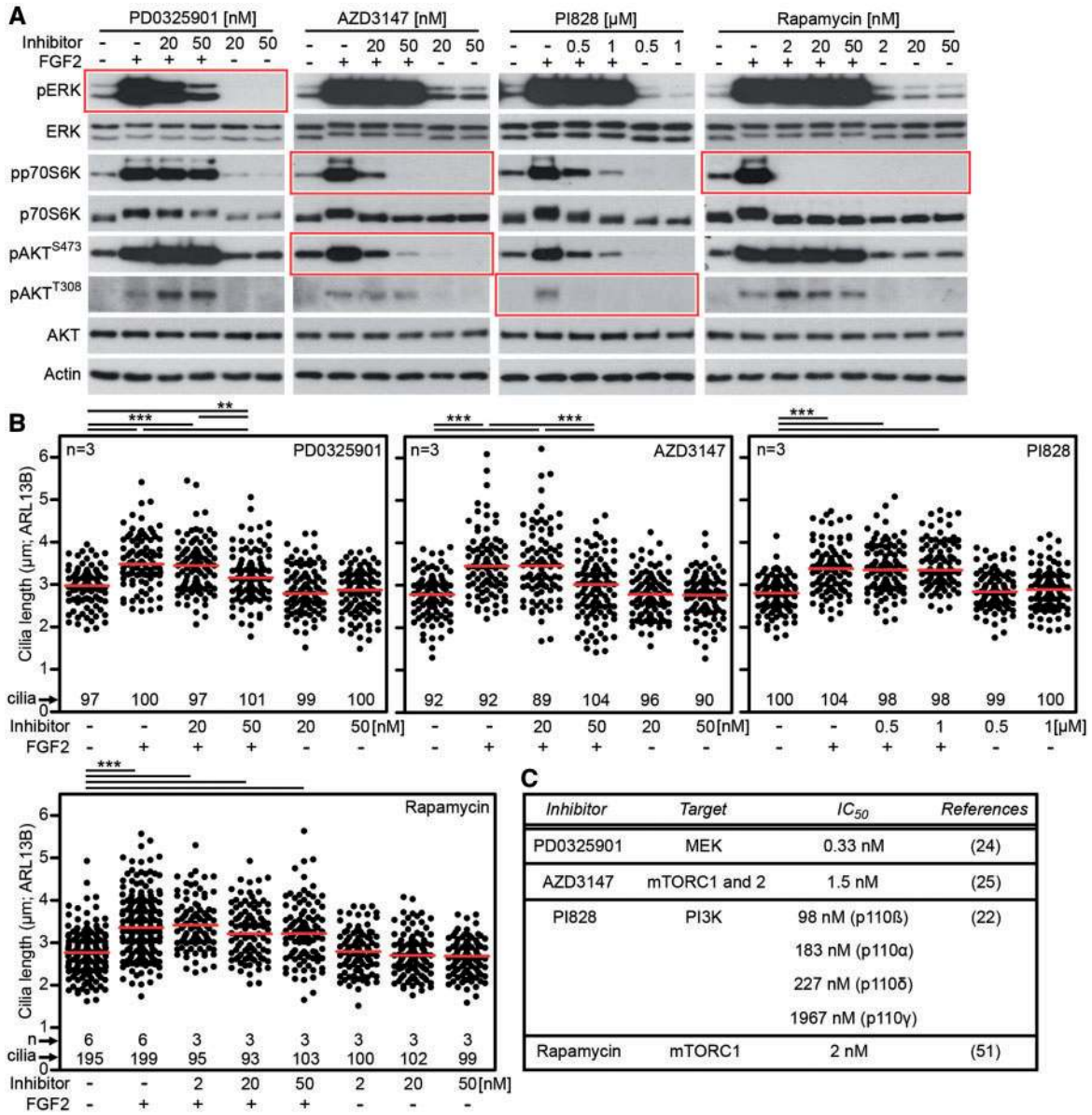

Figure 4. FGF signaling altered primary cilia via ERK and mTORC2 signaling. (**A**) NIH3T3 cells were treated with chemical inhibitors of MEK kinase (PD0325901), mTORC1/mTORC2 (AZD3147), PI3K (PI828) and mTORC1 (rapamycin) for 1 h prior to FGF2 treatment for 10 min. Inhibitor activity was confirmed by detection of phosphorylation (p) of targeted molecules in each inhibited pathway (indicated in red). Actin served as loading control. (**B**) NIH3T3 cells were treated with inhibitors and FGF2 for 12 h, the cilia were immunostained for ARL13B and their lengths were measured and plotted. Note that the inhibition of ERK pathway partially rescued FGF-mediated cilia elongation. Similar effect was achieved by mTORC1/mTORC2 inhibitor AZD3147. Rapamycin and PI828 showed no effect on FGF-mediated cilia elongation. (**C**) Published IC_{50} values for the inhibitors used.

direction. Plotting cilia lengths against the IFT velocities showed that cilia of different sizes moved IFT20-GFP faster in FGF-treated cells (Fig. 5D), demonstrating that measured differences in IFT speeds in control vs. FGF-treated cells were not biased by the differences in cilia length. A similar FGF-mediated increase in IFT speed was found in IMCD3 cells stably expressing IFT20-GFP (27) (Fig. 5F and G). These data establish that FGF-mediated increase of IFT velocity is not unique to NIH3T3 cells, or caused by possible artifacts generated by transient IFT20-GFP expression in these cells. Although a significant FGF effect on cargo frequency was found in NIH3T3 retrograde IFT, this was not reproduced in IMCD3 cells (Fig. 5E and H), suggesting that the regulation of IFT speed is the major process by which FGF affects primary cilia length.

Because the sustained activation of FGF signaling shortened primary cilia in contrast to extension observed for transient FGFR activation (Figs 1, 2 vs. 3), we asked whether this difference reflects also the differences in IFT speed. NIH3T3 cells were transfected with constitutively active FGFR3-K650E mutant, and the IFT speed was determined via IFT20-GFP kymographs. Expression of FGFR3-K650E slowed both anterograde and retrograde IFT (Fig. 5I), whilst the IFT20 frequency was downregulated only in the anterograde direction, with moderate statistical significance (Fig. 5K).

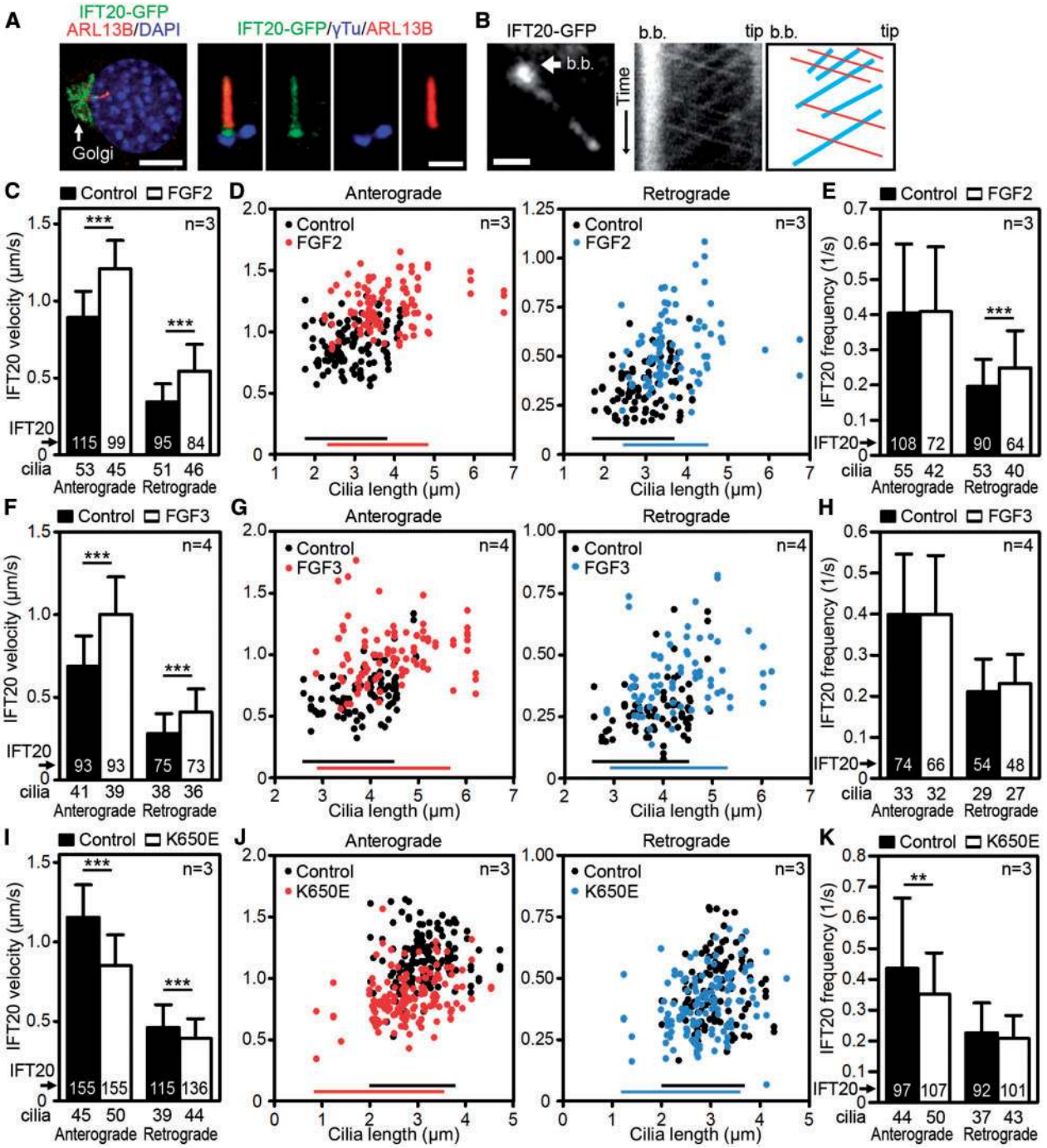

Figure 5. FGF signaling regulated IFT velocity in primary cilia. (**A**) NIH3T3 cells were transfected with IFT20-GFP and their cilia were counterstained with ARL13B/γ-tubulin (γTu) (scale bars 10 μm left, 1 μm right). (**B**) Cells were treated with FGF2 for 6–12 h, and kymographs were used to analyse IFT. IFT20-GFP-labelled cilia, b.b., basal body (left, scale bar 1 μm). Representative kymograph of IFT20-GFP with indicated basal body and tip of the cilium; red, anterograde trajectories, blue, retrograde trajectories (middle and right). (**C**, **D**) Analyses of velocity and frequency (**E**) of the IFT20-GFP cargo particles in cells treated with FGF2, compared with control (mean ± SD; Student's t-test, $^{**}P<0.01$, $^{***}P<0.001$). (D) FGF2 accelerates IFT independent of the cilia length. Anterograde (left) and retrograde (right) IFT20-GFP velocities were plotted against the lengths of the corresponding cilia; bars indicate $Q_{0.0}$-$Q_{0.9}$ of the cilia length. (**F**–**H**) Analyses of IFT velocities in IMCD3 cells stably transfected with IFT20-GFP demonstrated that similar to NIH3T3 cells (C–E), treatment with FGF3 accelerated IFT velocities while producing negligible effect on IFT frequency. (**I**–**K**) Analysis of IFT velocities in NIH3T3 cells transfected with IFT20-GFP together with the constitutively active FGFR3-K650E mutation demonstrated that constitutive activation of FGF signaling lowered IFT speed while producing negligible effect on IFT frequency.

FGF signaling interacts with Hh pathway

The translocation of SMO into the primary cilia is a prerequisite to activation of Hh signaling (4). Because SMO translocation depends on IFT (29) and FGF signaling affects IFT (Fig. 5), we determined the FGF effect on SMO localization into the cilia. Immunocytochemistry demonstrated SMO signal in nearly 100% of NIH3T3 cilia in the first 4 h after treatment with the SAG (SMO agonist), a small chemical activator of Hh

signaling (30). This phenotype was not affected by cell treatment with FGF2 (Fig. 6A). Quantification of SMO signal in the cilia however revealed significantly ($P < 0.001$) decreased intensity in cells treated with SAG and FGF2, when compared with cells treated with SAG only (Fig. 6A, right graph). In addition, FGF2 reduced levels of Hh target transcriptional regulator GLI3 at the tip of the cilia, in both control and SAG-treated cells (Supplementary Material, Fig. S1, arrow). The ratio of full-length (FL) and repressor (R) variants of GLI3 protein determines the nature of the cellular response to Hh pathway activation (31,32). In NIH3T3 cells, treatment with SAG triggered degradation of GLI3R, leading to altered GLI3FL/GLI3R ratio and induction of expression of Hh-target genes *Gli1* and *Ptch1* (Fig. 6B and C). FGF2 partially counteracted the SAG-mediated degradation of GLI3R, and corresponding induction of *Gli1* and *Ptch1* expression.

The expression of TD-associated FGFR3-K650M mutant in NIH3T3 cells affected Hh signaling similar to the treatment with FGF2 described above. First, SMO accumulation in cilia in response to SAG was nearly identical between the control and FGFR3-K650M expressing cells (Fig. 6D). Second, the FGFR3-K650M cells showed a significant reduction in amounts of ciliary SMO (Fig. 6D). Third, the SAG effect on GLI3 processing was partially suppressed in FGFR3-K650M cells, leading to impaired induction of GLI1 protein expression by SAG (Fig. 6E). Collectively, these data demonstrate that FGF signaling affects Hh pathway by interfering with the localization of SMO and GLI3 into the primary cilia. This leads to altered GLI3 processing in response to Hh activation, and attenuates induction of Hh responsive genes.

Discussion

The cilium serves as a primary signaling center for the Hh pathway, however it also regulates function of other pathways as part of cell-to-cell communication. For instance, while loss of primary cilia does not compromise Wnt signaling, it balances the magnitude of cell response to Wnt ligands, as evidenced by uncontrolled activation of canonical Wnt/β-catenin signaling in cells lacking primary cilia due to Kif3a deletion (33). Evidence is emerging that other signaling systems, which are not dependent on cilia as essential components of their pathways, require cilia for proper integration of their signaling into cells, or use cilia for cross-talk with Hh signaling. Here, we report interaction of FGF family of growth factors and morphogens with cilia.

Activation of FGF signaling affected the length of primary cilia in a total of 10 cell types examined here, including established cell lines of different origins (NIH3T3 fibroblasts, hESC and hiPSC and IMCD3 epithelial cells), primary mesenchymal cell lines (embryonic fibroblasts, mouse limb bud cells), human patient-derived cells (TD chondrocytes), *in vivo* mouse and human long bones (ACH and TD growth plate cartilage) and developing chick limb tissues. In addition, systemic inhibition of FGFR signaling resulted in shorter primary and motile cilia in mouse biliary ducts, proximal kidney tubuli and lung bronchi. Altogether, these data stablish that cilium is a common target of FGF signaling. This is further supported by evidence in lower vertebrates, where inactivation of FGF signaling lead to variations in cilia length across several *Xenopus* or zebrafish embryonal tissues (34). Thus the regulation of the ciliary length appears to be a functional component of canonical FGF signal transduction. Importantly, the cells and tissues analysed here differ significantly in their FGFR1–4 expression (Supplementary Material, Table S1), suggesting that the capacity to regulate cilia is unlikely restricted to individual FGFR. In another words, all four FGFRs target the common mechanism(s) of cilia regulation.

An interesting observation was that the anterior, but not the posterior region of the limb bud shows cilia shortening when stimulated with high dose of FGF2. Although there is no clear explanation for this phenotype, it may be caused by a higher sensitivity of an anterior limb bud mesechyme to FGF stimulus, as demonstrated by the absence of radius, but not ulna in chick limbs where endogenous FGF signaling was inhibited by chemical FGFR inhibitor (35). In addition, at the stage of limb bud development used here, the posterior limb bud exhibits high FGF ligand expression (FGF10 in the mesenchyme, FGF8 in the epithelium) compared with the anterior region (36). Overall, the data suggest that the anterior and posterior regions of early limb buds may differ in both the nature of cell response to FGF and in the mechanisms regulating primary cilia.

Our data point to a fine tuning of the cilia length by FGF signaling, manifested as two opposing phenotypes (Fig. 3F). First, experimental activation of transient FGF signaling extended primary cilia *in vitro*. Correspondingly, inhibition of physiological FGF signaling (which likely has a transient kinetics), resulted in shorter cilia *in vivo*, as evidenced in biliary ducts, kidney proximal tubuli and lung bronchi (mouse; this study), Kupffer's vesicle, pronephric ducts and otic vesicle (zebrafish), or gastrocoel roof plate (*Xenopus*) (34). Second, sustained activation of FGF signaling shortened primary cilia, as shown in FGF stimulated hESC or hiPSC, chicken limb buds injected with high dose of FGF2, ACH and TD chondrocytes expressing activating FGFR3 mutations or NIH3T3 fibroblasts expressing the activation TD FGFR3 mutant. Correspondingly, inhibition of sustained FGF signaling elongated primary cilia.

The data suggest that differences in kinetics of FGF signaling activation regulate primary cilia length in opposite ways, although this conclusion is limited by mostly descriptive, indirect comparison of kinetics of FGF signaling across different cell types. In NIH3T3 cells however, stimulation with FGF ligand activates FGF signaling for 8 h (37), compared with expression of constitutively active FGFR3 mutant, which activates FGF signaling for more than 24 h (Supplementary Material, Fig. S2). We demonstrate that both the cilia length and the IFT velocities are differently regulated by transient versus sustained activation of FGF signaling in NIH3T3. Future research should confirm whether the sustained FGF signaling affects primary cilia by regulating the same process targeted by transient FGF signaling, or by a distinct mechanism.

Cilia grow at their distal tips, where tubulin dimers are added to the plus ends of the microtubules. Because axoneme length reflects a balance between microtubule assembly and disassembly and is affected by the availability of free tubulins supplied by IFT (26), we hypothesized that one mechanism by which FGF signaling affects primary cilia is through regulation of IFT. Indeed, the opposite effects of FGF signaling on cilia length correlated with the changes in IFT velocity, such that increase in IFT velocities was induced by transient FGF signaling which extended cilia length, while sustained FGF signaling decreased both IFT speed and cilia length. These data demonstrate that regulation of IFT velocity represents one process through which the FGF signaling regulates primary cilia.

The exact mechanism(s) of FGF-mediated regulation of IFT and primary cilia length are not known. In NIH3T3 cells, chemical inhibition of MAKP/ERK and mTORC1 and 2, but not PI3K or mTORC1 alone, partially rescued the primary cilia extension caused by transient FGF signaling. These observations are in line with data demonstrating the role of mTOR activity in cilia

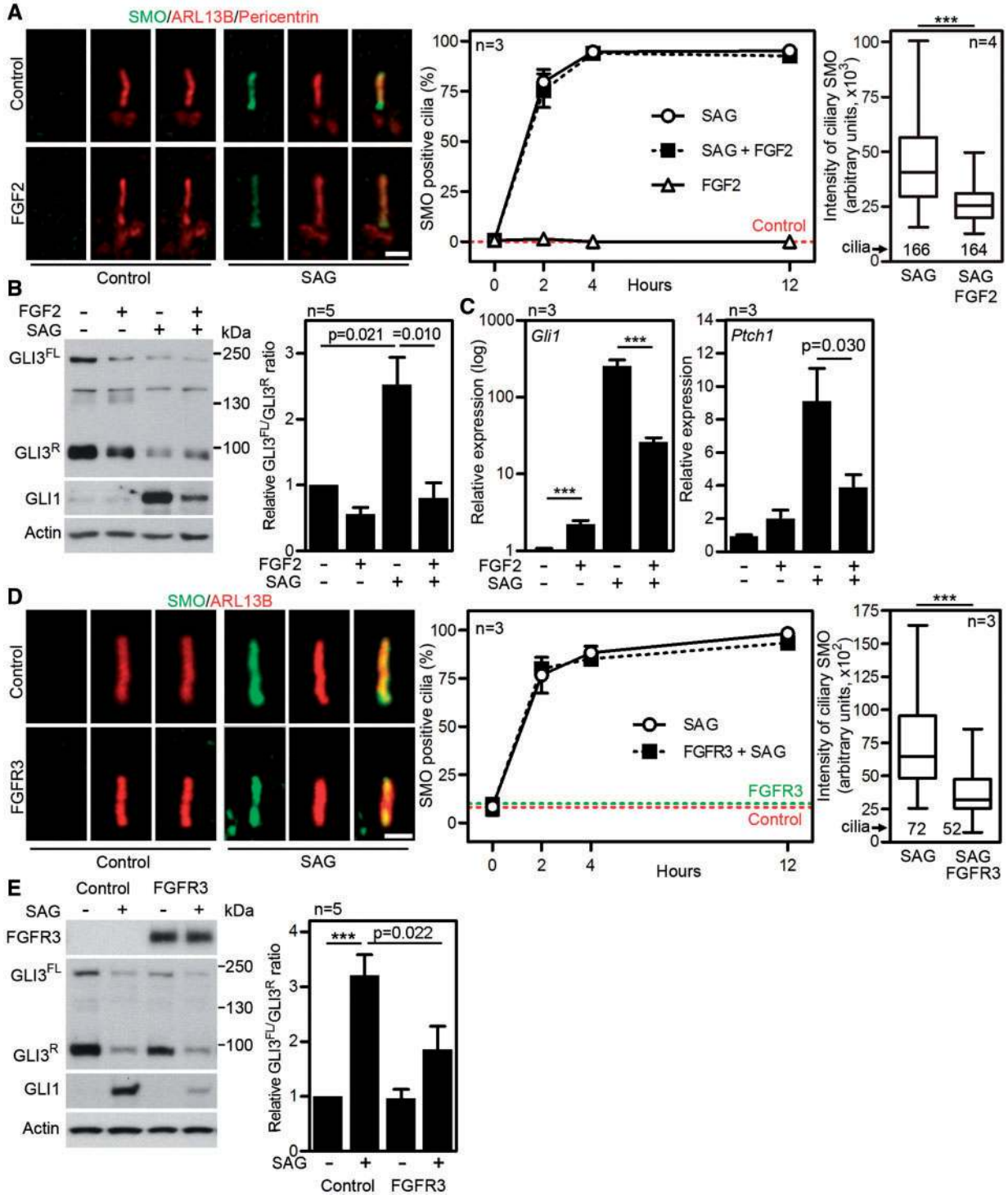

Figure 6. FGF signaling altered cellular response to Hh pathway activation. (A) NIH3T3 cells were treated with 2 ng/ml FGF2 and 500 nM SAG for 12 h or as indicated. Smoothened (SMO) was visualized by immunostaining (scale bar 1 μm), and the percentage of SMO-positive cilia were calculated and plotted (~300 cilia analysed for each time point) (middle). The SMO signal in the ciliary region defined by ARL13B signal was quantified and plotted. Box and whiskers, $Q_{0.25}$–$Q_{0.75}$ and $Q_{0.025}$–$Q_{0.975}$ of signal intensity; bar, median; Student's *t*-test (***$P<0.001$) (right). (B) Cells were treated as indicated for 12 h and immunoblotted for GLI1 and GLI3 (FL, full-length; R, repressor). The optical densities of $GLI3^{FL}$ and $GLI3^{R}$ were measured and plotted as a FL/R ratio relative to non-treated cells (mean ± SEM). (C) *Gli1* and *Ptch1* transcript levels in cells treated with FGF2 and SAG for 24 h were analysed by qPCR, and normalized to *Gapdh*. (D, E) NIH3T3 cells were transfected with the FGFR3-K650M mutation or an empty vector and treated with 500 nM SAG for 12 h. (D) SMO was visualized by immunostaining (scale bar 1 μm), and the percentage of SMO-positive cilia were calculated and plotted (60 cilia analysed for each time point) (middle). The SMO signal in ciliary region defined by ARL13B signal was quantified and plotted. Box and whiskers, $Q_{0.25}$–$Q_{0.75}$ and $Q_{0.025}$–$Q_{0.975}$ of signal intensity; bar, median (right). (E) Cells were immunoblotted for GLI1 and GLI3. The optical densities of $GLI3^{FL}$ and $GLI3^{R}$ were measured and plotted as a FL/R ratio relative to non-treated cells (mean ± SEM).

length regulation (38,39). Similarly, the ERK pathway has been described to regulate ciliary length, as demonstrated in zebrafish where the *fgfr1* morphants had shorter cilia and downregulated expression of the IFT genes *foxJ1*, *rfx2* and *polaris* (34). In chondrocytes and NIH3T3 cells, IL1 induced elongation of primary cilia that could be blocked by inhibition of MEK activity (40). Yet it is unclear to what extent the mTORC and ERK signaling participate in the FGF-cilia phenotypes described here. First, the mTORC inhibitor AZD3147 and ERK pathway inhibitor PD0325601 both rescued the FGF-mediated cilia extension at concentrations higher than their reported IC_{50} (Fig. 4C), suggesting off target activity. Second, it is not clear whether the cilia shortening mediated by sustained FGF signaling is a manifestation of differing or similar processes that extend primary cilia seen in transient FGF signaling. In contrast to our data on transient FGF signaling, a recent study by Martin et al. (2017) showed that in the model of sustained FGF signaling (mouse ACH and human TD chondrocytes), high dose rapamycin rescued the pathological cilia shortening. As the rapamycin concentration used was exceeding its reported IC_{50} (Fig. 4C), it leaves the question of the exact role of mTOR signaling in FGF-mediated cilia regulation opened for further investigation.

Several lines of evidence suggest that maintenance of proper ciliary length is critical for Hh signaling in cells. As an example, missense mutation in *IFT81*, a key component of the IFTB complex essential for anterograde transport, elongated cilia and disrupted Hh signaling (41). Similarly, reduced levels of DYNC2LI1 and DYNC2H1 components of the retrograde IFT motor dynein-2, resulted in cilia of variable length and impaired Hh signaling (42). In agreement with these data, we demonstrated that FGF-mediated alteration in cilia length correlates with altered Hh response. Specifically, activation of FGF signaling modified GLI3 processing and induction of Hh-responsive genes, triggered by cells treatment with the Hh pathway agonist SAG. Because SMO is necessary for Hh-induced GLI3 accumulation at the ciliary tip and its processing (5,43), it is likely that the less extensive translocation of SMO to primary cilia observed in cells with active FGF signaling resulted in a less pronounced response to SAG.

In vertebrate development, FGFR and Hh cooperate in regulation of patterning and growth of many organs, including the skeleton. First, in early limb bud mesenchyme, Shh produced by the posteriorly located zone of polarizing activity delivers antero-posterior patterning messages to govern digit identity (44). Simultaneously, signaling of at least five FGFs produced by mesenchyme and covering ectoderm regulate cell proliferation and limb bud outgrowth (45). Later in development when cartilage growth plates form, Indian hedgehog (Ihh) acts as a chondrocyte mitogen, regulating chondrocyte proliferation and differentiation (46). Abnormal Ihh signaling was demonstrated in mouse models in FGFR3-related skeletal dysplasias, including ACH mice expressing the FGFR3-G380R, mice expressing p.G369C activating FGFR3 mutation (corresponding to human TD1 mutation p.G370C) or mice expressing the FGFR3-K644E mutation (corresponding to human TD2 mutation p.K650E) (11,12,47). Our findings of aberrant cilia in ACH and TD growth plates identify both conditions as ciliopathies. Furthermore, we demonstrated that cilia dysregulation in ACH and TD chondrocytes stems from direct FGFR3 action, thus opening a possibility that defective cilia-Hh signaling plays role in the pathology of the FGFR3-related skeletal dysplasia. While not a straightforward on or off switch, our data identified different ciliary responses with transient versus sustained FGF signaling, and these findings should be considered in the development of FGFR therapeutics, several of which are currently in clinical trials (48).

Materials and Methods

Cell culture, vectors and transfection, and qPCR

NIH3T3 cells were obtained from ATCC (Manassas, VA). Human control and TD chondrocytes (International Skeletal Dysplasia Registry Numbers. 90–028, 00–082, 93–064B, 02–137, 12–371A, 14–005 and 97–001) were obtained under an approved UCLA human subjects protocol. Cells were propagated in DMEM media, supplemented with 10% FBS and antibiotics (Invitrogen, Carlsbad, CA). IFT20-GFP expressing IMCD3 cells were previously described (27), and propagated in DMEM: F12 (1:1) media supplemented with 10% FBS and 500 μg/ml G418 (Invitrogen). CCTL14 and AM13 were propagated as feeder-independent monolayers. Cells were starved in the presence of 0.1% FBS (NIH3T3) or without serum (IMCD3, chondrocytes, CCTL14 and AM13). FGF2, FGF3, FGF7 and FGF10 were obtained from RnD Systems (Minneapolis, MN), AZD4547 from Selleckchem (Houston, TX); PD0325901, PI828, AZD3147 and rapamycin were from Tocris (Bristol, UK), and SAG from Millipore (Billerica, MA). Cells were transfected using the FuGENE6 reagent (Promega, Madison, WI) or Lipofectamine (Invitrogen). Vector human full-length FGFR3 was described elsewhere (49); IFT20-GFP vector was a kind gift from Gregory Pazour (University of Massachusetts Medical School, Worcester, MA). Total RNA was isolated using RNeasy Mini Kit (Qiagen, Hilden, DE) and reverse transcription performed using the First Strand cDNA Synthesis Kit (Roche, Basel, Switzerland). For qPCR, the following QuantiTect Primers were utilized (Qiagen): Mm_Ptch1_1_SG (QT00149135), Mm_Gli1_1_SG (QT00173537), Mm_Gapdh_3_SG (QT01658692).

Western blot

Cells were harvested directly into the sample buffer (4% SDS, 20% glycerol, 10% β-mercaptoethanol, 0.02% bromophenol blue, 125 mM TRIS-HCl pH 6.8). Cell lysates were resolved by SDS-PAGE, transferred onto a PVDF membrane and visualized by chemiluminiscence (Thermo Scientific, Rockford, IL). Protein band intensities were quantified in ImageJ (http://imagej.nih.gov/ij/). The following antibodies were used: $pAKT^{T308}$ (9275), $pAKT^{S473}$ (4060), AKT (4691), $pERK^{T202/Y204}$ (4376), ERK (9102), $pFRS2^{Y436}$ (3861), GLI1 (2643), $pS6K1^{T389}$ (9205), S6K1 (9202), actin (3700; Cell Signaling, Beverly, MA); FRS2 (sc-8318), $pFGFR3^{Y724}$ (sc-33041; Santa Cruz Biotechnology, Santa Cruz, CA); FLAG (F1804); V5 (R960–25; Invitrogen), GLI3 (AF3690; RnD Systems), tubulin (11–250; Exbio, Prague, CZE).

Immunocytochemistry and measurements of cilia length, IFT and SMO

Cells were fixed in paraformaldehyde, post-fixed in ice-cold methanol if γ-tubulin was interrogated, and incubated with the following antibodies: acetylated α-tubulin (32–2700; Invitrogen), FLAG (F1804; Sigma-Aldrich, St. Louis, MO), ARL13B (17711–1-AP; Proteintech, Rosemont, IL), γ-tubulin (ab11316), pericentrin (ab4448; Abcam, Cambridge, UK), GLI3 (AF3690; RnD Systems); V5 (sc-83849), Oct4 (sc-8629) and SMO (sc-166685; Santa-Cruz). Secondary antibodies conjugated with AlexaFluor488/594 and AlexaFluor405 were from Invitrogen and Abcam, respectively. Measurements of cilia length in 3D were performed as previously described (50). IFT20-GFP velocities were measured using Carl Zeiss LSM 700 equipped with an atmospheric chamber. Fast time-lapse microscopy videos of individual cilia were obtained, and the data were processed using Multi Kymograph

plugin (Jens Rietdorf and Arne Seitz) in Fiji. Kymographs were used to calculate the IFT velocity by manual measurements of the slopes of visible signal curves. The kymograph lines were also used to calculate the IFT20 frequency, as the vertical distances of two neighboring lines representing time periods between the two travelling IFTs. The intensity of ciliary SMO was analysed using maximal projections of Z-stacks in Fiji. The ARL13B signal was used to manually outline the ciliary region, and the SMO signal was measured as a total sum of the fluorescence signal intensity.

Animal experiments, histology and immunohistochemistry

Mouse embryonic fibroblasts were isolated from E12.5 CF-1 mice by trypsinization of the embryo after the head and internal organs were removed. Fertilized chicken eggs (ISA brown) were obtained from Integra (Zabcice, CZE), incubated in a humidified forced air incubator at 37.8°C and FGF2 (1 mg/ml) was injected into the right-wing bud using a micromanipulator (Leica, Wetzlar, DE) and microinjector (Eppendorf, Hamburg, DE). Left wings were injected with the FGF2 vehicle phosphate-buffered saline. Embryos were collected 24 h after injection, fixed in paraformaldehyde and paraffin embedded limb buds were sectioned at a thickness of 5 μm. The sections were deparaffinised, rehydrated, treated with hydrogen peroxide to eliminate endogenous peroxidase activity, pre-treated in citrate buffer and stained for ARL13B. To produce micromasses, primary mesenchymal cells were harvested from the limb buds of E12 mouse embryos, digested with dispase II to obtain single cell suspensions and spotted in 10 μl aliquots at 2×10^7 cells/ml. Spots were left for cells to adhere for 1.5 h before differentiating media (60% F12/40% DMEM with 10% FBS supplemented with 50 μg/ml ascorbic acid, 10 mM β-glycerol phosphate, 1% L-glutamine and 1% penicillin/streptomycin) was added. Micromasses were grown for 1 day in media supplemented with FGF2 (Sigma-Aldrich), fixed with paraformaldehyde and stained with hematoxylin or further processed for cilia immunostaining. For cilia imaging, cells were fixed with methanol and subsequently with paraformaldehyde, and immunolabeled by ARL13B and γ-tubulin (T6557, Sigma-Aldrich) antibodies. Stained primary cilia were imaged using the Carl Zeiss LSM780 microscope. For *in vivo* AZD4547 experiments, the newborn CD1 mice were intraperitoneally injected with 1 mM AZD4547 or its vehicle DMSO as previously described (19). Mice were euthanized by cervical dislocation in accordance with the AVMA Guidelines on Euthanasia. Liver, kidney and lung were fixed in paraformaldehyde and embedded in paraffin, and 5 μm sections were stained with hematoxylin/eosin or with antibodies for acetylated tubulin and pericentrin. The tibias from ACH (*Fgfr3*$^{G369C/+}$) and wild-type mice were fixed with paraformaldehyde, decalcified, wrapped and sectioned (10 μm). Frozen sections were immunolabeled for acetylated tubulin, and imaged using the Carl Zeiss LSM880 microscope. Animal experiments were reviewed and approved by the Laboratory Animal Welfare and Ethics Committee of the Third Military Medical University (Chongqing, China) and the Institutional Animal Care and Use Committee at the Institute of Animal Physiology and Genetics, Czech Academy of Sciences (Libechov, Czech Republic; 144/2013). Distal femurs obtained from probands with thanatophoric dysplasia probands were obtained from the gestational ages of 16 to 20 weeks. Femora including the cartilage growth plate and were cut vertically for more efficient processing, fixed in 4% paraformaldehyde, decalcified, dehydrated and embedded in paraffin. For histology, the 10 μm sections were stained by picrosirius red and hematoxylin. The primary cilia were immunostained with ARL13B antibody.

Statistical analyses

All experiments were performed at least in triplicates unless stated otherwise. The n values express the actual number of independent biological experiments. Data are presented as mean ± SEM unless stated otherwise. Two-tailed Student's *t*-test was used for statistical evaluation of differences.

Supplementary Material

Supplementary Material is available at *HMG* online.

Acknowledgements

We also thank the March of Dimes and the Joseph Drown Foundation for their support of the International Skeletal Dysplasia Registry.

Conflict of Interest statement. None declared

Funding

National Program of Sustainability II (MEYS CR; Project no. LQ1605); Ministry of Education, Youth and Sports of the Czech Republic (KONTAKT II LH15231); Operational Programme Research, Development and Education (CZ.02.1.01/0.0/0.0/15_003/0000460); Agency for Healthcare Research of the Czech Republic (15–33232A, 15–34405A); Czech Science Foundation (GA17–09525S; GA15–23033S); National Natural Science Foundation of China (81530071). DK is supported by NIH grants R01AR062651, RO1AR066124 and RO1DE019567, and NIH/National Center for Advancing Translational Science (NCATS) UCLA CTSI Grant Number UL1TR000124. MKB was supported by Junior Researcher Award from the Faculty of Medicine, Masaryk University.

References

1. Lechtreck, K.F. (2015) IFT-cargo interactions and protein transport in cilia. *Trends Biochem. Sci.*, **40**, 765–778.
2. Goetz, S.C. and Anderson, K.V. (2010) The primary cilium: a signalling centre during vertebrate development. *Nat. Rev. Genet.*, **11**, 331–344.
3. Huangfu, D., Liu, A., Rakeman, A.S., Murcia, N.S., Niswander, L. and Anderson, K.V. (2003) Hedgehog signalling in the mouse requires intraflagellar transport proteins. *Nature*, **426**, 83–87.
4. Corbit, K.C., Aanstad, P., Singla, V., Norman, A.R., Stainier, D.Y.R. and Reiter, J.F. (2005) Vertebrate Smoothened functions at the primary cilium. *Nature*, **437**, 1018–1021.
5. Tukachinsky, H., Lopez, L.V. and Salic, A. (2010) A mechanism for vertebrate Hedgehog signaling: recruitment to cilia and dissociation of SuFu-Gli protein complexes. *J. Cell Biol.*, **191**, 415–428.
6. Dai, P., Akimaru, H., Tanaka, Y., Maekawa, T., Nakafuku, M. and Ishii, S. (1999) Sonic Hedgehog-induced activation of the Gli1 promoter is mediated by GLI3. *J. Biol. Chem.*, **274**, 8143–8152.

7. Bowers, M., Eng, L., Lao, Z., Turnbull, R.K., Bao, X., Riedel, E., Mackem, S. and Joyner, A.L. (2012) Limb anterior-posterior polarity integrates activator and repressor functions of GLI2 as well as GLI3. *Dev. Biol.*, **370**, 110–124.
8. Itoh, N. and Ornitz, D.M. (2011) Fibroblast growth factors: from molecular evolution to roles in development, metabolism and disease. *J. Biochem.*, **149**, 121–130.
9. Bonafe, L., Cormier-Daire, V., Hall, C., Lachman, R., Mortier, G., Mundlos, S., Nishimura, G., Sangiorgi, L., Savarirayan, R., Sillence, D. *et al.* (2015) Nosology and classification of genetic skeletal disorders: 2015 revision. *Am. J. Med. Genet. Part A*, **167**, 2869–2892.
10. Foldynova-Trantirkova, S., Wilcox, W.R. and Krejci, P. (2012) Sixteen years and counting: the current understanding of fibroblast growth factor receptor 3 (FGFR3) signaling in skeletal dysplasias. *Hum. Mutat.*, **33**, 29–41.
11. Chen, L., Li, C., Qiao, W., Xu, X. and Deng, C. (2001) A Ser(365)–>Cys mutation of fibroblast growth factor receptor 3 in mouse downregulates Ihh/PTHrP signals and causes severe achondroplasia. *Hum. Mol. Genet.*, **10**, 457–465.
12. Chen, L., Adar, R., Yang, X., Monsonego, E.O., Li, C., Hauschka, P.V., Yayon, A. and Deng, C.X. (1999) Gly369Cys mutation in mouse FGFR3 causes achondroplasia by affecting both chondrogenesis and osteogenesis. *J. Clin. Invest.*, **104**, 1517–1525.
13. Gavine, P.R., Mooney, L., Kilgour, E., Thomas, A.P., Al-Kadhimi, K., Beck, S., Rooney, C., Coleman, T., Baker, D., Mellor, M.J. *et al.* (2012) AZD4547: an orally bioavailable, potent, and selective inhibitor of the fibroblast growth factor receptor tyrosine kinase family. *Cancer Res.*, **72**, 2045–2056.
14. Sheeba, C.J., Andrade, R.P., Duprez, D. and Palmeirim, I. (2010) Comprehensive analysis of fibroblast growth factor receptor expression patterns during chick forelimb development. *Int. J. Dev. Biol.*, **54**, 1517–1526.
15. Buchtova, M., Chaloupkova, R., Zakrzewska, M., Vesela, I., Cela, P., Barathova, J., Gudernova, I., Zajickova, R., Trantirek, L., Martin, J. *et al.* (2015) Instability restricts signaling of multiple fibroblast growth factors. *Cell. Mol. Life Sci.*, **72**, 2445–2459.
16. Dvorak, P., Dvorakova, D., Koskova, S., Vodinska, M., Najvirtova, M., Krekac, D. and Hampl, A. (2005) Expression and potential role of fibroblast growth factor 2 and its receptors in human embryonic stem cells. *Stem Cells*, **23**, 1200–1211.
17. Eiselleova, L., Matulka, K., Kriz, V., Kunova, M., Schmidtova, Z., Neradil, J., Tichy, B., Dvorakova, D., Pospisilova, S., Hampl, A. *et al.* (2009) A complex role for FGF-2 in self-renewal, survival, and adhesion of human embryonic stem cells. *Stem Cells*, **27**, 1847–1857.
18. Vanova, T., Konecna, Z., Zbonakova, Z., La Venuta, G., Zoufalova, K., Jelinkova, S., Varecha, M., Rotrekl, V., Krejci, P., Nickel, W. *et al.* (2017) Tyrosine kinase expressed in hepatocellular carcinoma, TEC, controls pluripotency and early cell fate decisions of human pluripotent stem cells via regulation of fibroblast growth factor-2 secretion. *Stem Cells*, **35**, 2050–2059.
19. Gudernova, I., Vesela, I., Balek, L., Buchtova, M., Dosedelova, H., Kunova, M., Pivnicka, J., Jelinkova, I., Roubalova, L., Kozubik, A. *et al.* (2016) Multikinase activity of fibroblast growth factor receptor (FGFR) inhibitors SU5402, PD173074, AZD1480, AZD4547 and BGJ398 compromises the use of small chemicals targeting FGFR catalytic activity for therapy of short-stature syndromes. *Hum. Mol. Genet.*, **25**, 9–23.
20. Garcia-Maya, M., Anderson, A.A., Kendal, C.E., Kenny, A.V., Edwards-Ingram, L.C., Holladay, A. and Saffell, J.L. (2006) Ligand concentration is a driver of divergent signaling and pleiotropic cellular responses to FGF. *J. Cell. Physiol.*, **206**, 386–393.
21. Ornitz, D.M., Xu, J., Colvin, J.S., McEwen, D.G., MacArthur, C.A., Coulier, F., Gao, G. and Goldfarb, M. (1996) Receptor specificity of the fibroblast growth factor family. *J. Biol. Chem.*, **271**, 15292–15297.
22. Gharbi, S.I., Zvelebil, M.J., Shuttleworth, S.J., Hancox, T., Saghir, N., Timms, J.F. and Waterfield, M.D. (2007) Exploring the specificity of the PI3K family inhibitor LY294002. *Biochem. J.*, **404**, 15–21.
23. Mukhopadhyay, S., Frias, M.A., Chatterjee, A., Yellen, P. and Foster, D.A. (2016) The enigma of rapamycin dosage. *Mol. Cancer Ther.*, **15**, 347–353.
24. Barrett, S.D., Bridges, A.J., Dudley, D.T., Saltiel, A.R., Fergus, J.H., Flamme, C.M., Delaney, A.M., Kaufman, M., LePage, S., Leopold, W.R. *et al.* (2008) The discovery of the benzhydroxamate MEK inhibitors CI-1040 and PD 0325901. *Bioorg. Med. Chem. Lett.*, **18**, 6501–6504.
25. Pike, K.G., Morris, J., Ruston, L., Pass, S.L., Greenwood, R., Williams, E.J., Demeritt, J., Culshaw, J.D., Gill, K., Pass, M. *et al.* (2015) Discovery of AZD3147: a potent, selective dual inhibitor of mTORC1 and mTORC2. *J. Med. Chem.*, **58**, 2326–2349.
26. Marshall, W.F., Qin, H., Rodrigo Brenni, M. and Rosenbaum, J.L. (2005) Flagellar length control system: testing a simple model based on intraflagellar transport and turnover. *Mol. Biol. Cell*, **16**, 270–278.
27. Broekhuis, J.R., Verhey, K.J. and Jansen, G. (2014) Regulation of cilium length and intraflagellar transport by the RCK-kinases ICK and MOK in renal epithelial cells. *PLoS One*, **9**, e108470.
28. Follit, J.A., Tuft, R.A., Fogarty, K.E. and Pazour, G.J. (2006) The intraflagellar transport protein IFT20 is associated with the golgi complex and is required for cilia assembly. *Mol. Biol. Cell*, **17**, 3781–3792.
29. Wang, Y., Zhou, Z., Walsh, C.T. and McMahon, A.P. (2009) Selective translocation of intracellular Smoothened to the primary cilium in response to Hedgehog pathway modulation. *Proc. Natl. Acad. Sci. U. S. A*, **106**, 2623–2628.
30. Chen, J.K., Taipale, J., Young, K.E., Maiti, T. and Beachy, P.A. (2002) Small molecule modulation of Smoothened activity. *Proc. Natl. Acad. Sci.*, **99**, 14071–14076.
31. Huangfu, D. and Anderson, K.V. (2005) Cilia and Hedgehog responsiveness in the mouse. *Proc. Natl. Acad. Sci.*, **102**, 11325–11330.
32. Humke, E.W., Dorn, K.V., Milenkovic, L., Scott, M.P. and Rohatgi, R. (2010) The output of Hedgehog signaling is controlled by the dynamic association between Suppressor of Fused and the Gli proteins. *Genes Dev.*, **24**, 670–682.
33. Corbit, K.C., Shyer, A.E., Dowdle, W.E., Gaulden, J., Singla, V., Reiter, J.F., Chuang, P.-T. and Reiter, J.F. (2008) Kif3a constrains β-catenin-dependent Wnt signalling through dual ciliary and non-ciliary mechanisms. *Nat. Cell Biol.*, **10**, 70–76.
34. Neugebauer, J.M., Amack, J.D., Peterson, A.G., Bisgrove, B.W. and Yost, H.J. (2009) FGF signalling during embryo development regulates cilia length in diverse epithelia. *Nature*, **458**, 651–654.
35. Horakova, D., Cela, P., Krejci, P., Balek, L., Moravcova Balkova, S., Matalova, E. and Buchtova, M. (2014) Effect of FGFR inhibitors on chicken limb development. *Dev. Growth Differ.*, **56**, 555–572.

36. Darnell, D.K., Kaur, S., Stanislaw, S., Davey, S., Konieczka, J.H., Yatskievych, T.A. and Antin, P.B. (2007) GEISHA: an in situ hybridization gene expression resource for the chicken embryo. *Cytogenet. Genome Res.*, **117**, 30–35.
37. Ekerot, M., Stavridis, M.P., Delavaine, L., Mitchell, M.P., Staples, C., Owens, D.M., Keenan, I.D., Dickinson, R.J., Storey, K.G. and Keyse, S.M. (2008) Negative-feedback regulation of FGF signalling by DUSP6/MKP-3 is driven by ERK1/2 and mediated by Ets factor binding to a conserved site within the DUSP6/MKP-3 gene promoter. *Biochem. J.*, **412**, 287–298.
38. Cardenas-Rodriguez, M., Irigoín, F., Osborn, D.P.S., Gascue, C., Katsanis, N., Beales, P.L. and Badano, J.L. (2013) The Bardet–Biedl syndrome-related protein CCDC28B modulates mTORC2 function and interacts with SIN1 to control cilia length independently of the mTOR complex. *Hum. Mol. Genet.*, **22**, 4031–4042.
39. Yuan, S., Li, J., Diener, D.R., Choma, M.A., Rosenbaum, J.L. and Sun, Z. (2012) Target-of-rapamycin complex 1 (Torc1) signaling modulates cilia size and function through protein synthesis regulation. *Proc. Natl. Acad. Sci.USA*, **109**, 2021–2026.
40. Wann, A.K.T. and Knight, M.M. (2012) Primary cilia elongation in response to interleukin-1 mediates the inflammatory response. *Cell. Mol. Life Sci.*, **69**, 2967–2977.
41. Duran, I., Taylor, S.P., Zhang, W., Martin, J., Forlenza, K.N., Spiro, R.P., Nickerson, D.A., Bamshad, M., Cohn, D.H. and Krakow, D. (2016) Destabilization of the IFT-B cilia core complex due to mutations in IFT81 causes a Spectrum of Short-Rib Polydactyly Syndrome. *Sci. Rep.*, **6**, 34232.
42. Taylor, S.P., Dantas, T.J., Duran, I., Wu, S., Lachman, R.S., Bamshad, M.J., Shendure, J., Nickerson, D.A., Nelson, S.F., Cohn, D.H. *et al.* (2015) Mutations in DYNC2LI1 disrupt cilia function and cause short rib polydactyly syndrome. *Nat. Commun.*, **6**, 7092.
43. Niewiadomski, P., Kong, J.H., Ahrends, R., Ma, Y., Humke, E.W., Khan, S., Teruel, M.N., Novitch, B.G. and Rohatgi, R. (2014) Gli Protein activity is controlled by multisite phosphorylation in vertebrate Hedgehog signaling. *Cell Rep*, **6**, 168–181.
44. te Welscher, P., Zuniga, A., Kuijper, S., Drenth, T., Goedemans, H.J., Meijlink, F. and Zeller, R. (2002) Progression of vertebrate limb development through SHH-mediated counteraction of GLI3. *Science*, **298**, 827–830.
45. Teven, C.M., Farina, E.M., Rivas, J. and Reid, R.R. (2014) Fibroblast growth factor (FGF) signaling in development and skeletal diseases. *Genes Dis.*, **1**, 199–213.
46. Vortkamp, A., Lee, K., Lanske, B., Segre, G.V., Kronenberg, H.M. and Tabin, C.J. (1996) Regulation of rate of cartilage differentiation by Indian hedgehog and PTH-related protein. *Science*, **273**, 613–622.
47. Li, C., Chen, L., Iwata, T., Kitagawa, M., Fu, X.Y. and Deng, C.X. (1999) A Lys644Glu substitution in fibroblast growth factor receptor 3 (FGFR3) causes dwarfism in mice by activation of STATs and ink4 cell cycle inhibitors. *Hum. Mol. Genet.*, **8**, 35–44.
48. Tanner, Y. and Grose, R.P. (2016) Dysregulated FGF signalling in neoplastic disorders. *Semin. Cell Dev. Biol.*, **53**, 126–135.
49. Krejci, P., Aklian, A., Kaucka, M., Sevcikova, E., Prochazkova, J., Masek, J.K., Mikolka, P., Pospisilova, T., Spoustova, T., Weis, M. *et al.* (2012) Receptor tyrosine kinases activate canonical WNT/β-catenin signaling via MAP kinase/LRP6 pathway and direct β-catenin phosphorylation. *PLoS One*, **7**, e35826.
50. Paige Taylor, S., Kunova Bosakova, M., Varecha, M., Balek, L., Barta, T., Trantirek, L., Jelinkova, I., Duran, I., Vesela, I., Forlenza, K.N. *et al.* (2016) An inactivating mutation in intestinal cell kinase, ICK, impairs hedgehog signalling and causes short rib-polydactyly syndrome. *Hum. Mol. Genet.*, **25**, 3998–4011.
51. Toral-Barza, L., Zhang, W.G., Lamison, C., Larocque, J., Gibbons, J. and Yu, K. (2005) Characterization of the cloned full-length and a truncated human target of rapamycin: activity, specificity, and enzyme inhibition as studied by a high capacity assay. *Biochem. Biophys. Res. Commun.*, **332**, 304–310.